#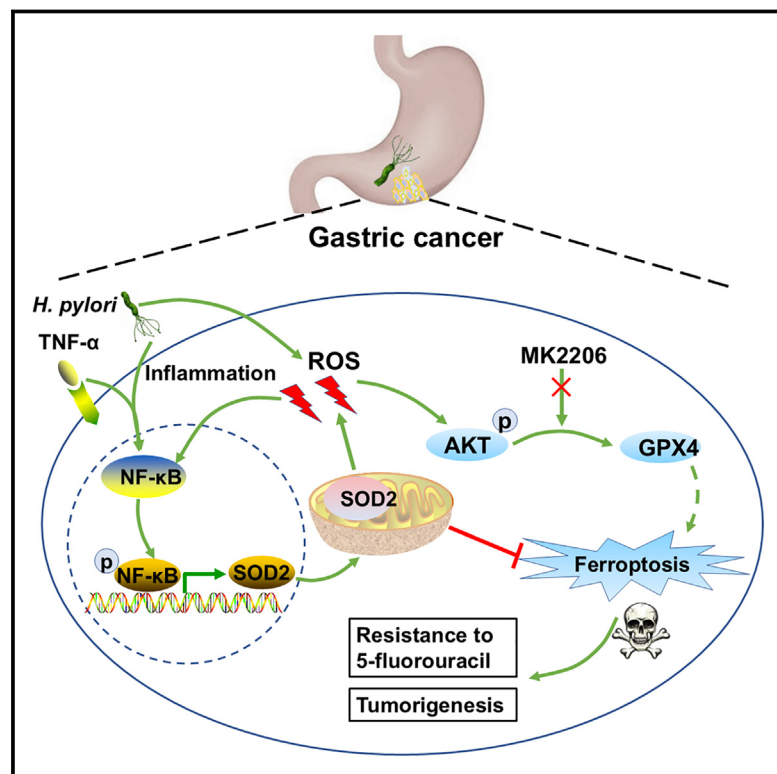 Superoxide dismutase promotes gastric tumorigenesis mediated by *Helicobacter pylori* and enhances resistance to 5-fluorouracil in gastric cancer

Graphical abstract

Authors

Hongbing Fu, Yu Zhang, Yantao Duan, ..., Qing You, Ronglin Yan, Weijun Wang

Correspondence

yanronglin@smmu.edu.cn (R.Y.), wweijun2023@163.com (W.W.)

In brief

Molecular biology; Cancer

Highlights

- SOD2 is upregulated in gastric cancer (GC) and predicts a poor prognosis

- *H. pylori* infection induces increased expression of SOD2 by activating NF-κB

- *H. pylori* regulates the redox status of GC by modulating SOD2/GPX4 expression

- SOD2 inhibits the ferroptosis and inhibition of SOD2 sensitizes GC to 5-FU treatment

CellPress

iScience

Article

Superoxide dismutase promotes gastric tumorigenesis mediated by *Helicobacter pylori* and enhances resistance to 5-fluorouracil in gastric cancer

Hongbing Fu,[1,5] Yu Zhang,[1,2,3,5] Yantao Duan,[3,4,5] Xin Zhang,[1] Jun Yao,[1] Dejun Yang,[1] Ziran Wei,[1] Zhenxin Zhu,[1] Jiapeng Xu,[1] Zunqi Hu,[1] Qing You,[1] Ronglin Yan,[1,*] and Weijun Wang[1,6,*]

[1]Department of Gastrointestinal Surgery, Changzheng Hospital, Naval Medical University (Second Military Medical University), Shanghai, China
[2]Department of Colorectal Surgery, Fudan University Shanghai Cancer Center, Shanghai, China
[3]Department of Oncology, Shanghai Medical College, Fudan University, Shanghai, China
[4]Department of Gastric Surgery, Fudan University Shanghai Cancer Center, Shanghai, China
[5]These authors contributed equally
[6]Lead contact
*Correspondence: yanronglin@smmu.edu.cn (R.Y.), wweijun2023@163.com (W.W.)
https://doi.org/10.1016/j.isci.2024.111553

SUMMARY

Helicobacter pylori (*H. pylori*) infection is the most common risk factor for gastric cancer (GC). The effect of the antioxidase manganese superoxide dismutase (SOD2) in gastric tumorigenesis remains unclear. We explored the molecular mechanisms of links between *H. pylori*, inflammation, and SOD2 in GC. We found that SOD2 was upregulated in GC. GC patients with high SOD2 expression showed worse overall survival. *H. pylori* infection promoted SOD2 expression by transcriptionally activating the NF-κB signaling pathway. Knockdown of SOD2 led to increased levels of reactive oxygen species and oxidative stress in response to *H. pylori* infection. Our research demonstrates that SOD2 can serve as an inhibitor of ferroptosis by activating AKT, and stabilizing GPX4 protein, which subsequently induces 5-fluorouracil resistance. These findings reveal a mechanism whereby *H. pylori* can promote gastric carcinogenesis by activating the NF-κB/SOD2/AKT/GPX4 pathway, leading to the inhibition of ferroptosis. This may provide a promising therapeutic target for GC.

INTRODUCTION

In 2020, gastric cancer (GC) was the fifth most common cancer and the fourth leading cause of cancer-related deaths worldwide.[1] *Helicobacter pylori* (*H. pylori*) infection was identified as a class I carcinogen by the World Health Organization in 1994 and is a major risk factor for GC.[2,3] Infection with *H. pylori* leads to abnormal host inflammatory responses, which result in chronic inflammation and atrophic gastritis that may develop into GC.[4] The chronic inflammatory environment correlates with increased levels of reactive oxygen species (ROS), resulting in the activation of oncogenic pathways that participate in *H. pylori*-induced gastric tumorigenesis.[5,6]

Manganese superoxide dismutase (SOD2), which is a mitochondrial antioxidant enzyme, regulates the disproportionation of locally generated free radicals.[7] It converts these free radicals into hydrogen peroxide, which is further detoxified into water for cell survival by glutathione peroxidases (GPx) or peroxiredoxins (Prxs) and is involved in the maintenance of cellular ROS homeostasis.[8] Optimal protection can be achieved if a reasonable balance of oxidoreductase enzymes is well sustained. Recent studies have found that high ratios of SOD2/GPx1 may lead to

increased levels of H_2O_2 in mitochondria. Accumulation of free radicals correlates with mitochondrial dysfunction, progression, and metastasis in aggressive tumors.[9] Growing evidence suggests that SOD2 can serve as both a tumor suppressor and an oncogene. Reduced SOD2 expression was detected in pancreatic cancer, and SOD2 significantly inhibited tumor cell growth by enhancing cell cycle progression with increased ROS levels.[10] Loss of SOD2 can also result in ROS-induced DNA damage and further lead to cellular transformation and carcinogenesis.[11]

Although SOD2 is downregulated in the early stages of tumorigenesis, Hemachandra et al. reported that SOD2 was overexpressed in metastatic tumor lesions and aggressive tumors.[12] SOD2 elevates the ratios of cellular oxidants/antioxidants, playing a direct role in tumor progression.[13] Furthermore, the binding of Ets-1 to the matrix metalloproteinase-1 (MMP-1) promoter region and the maintenance of c-Jun N-terminal kinase (JNK) pathway activation require the enzymatic activity of SOD2.[14] SOD2 is essential for the stimulation of MMP-1 through the H_2O_2-dependent regulation of the mitogen-activated protein kinase (MAPK) pathway, resulting in the remodeling of the extracellular matrix and thereby promoting tumor invasion and
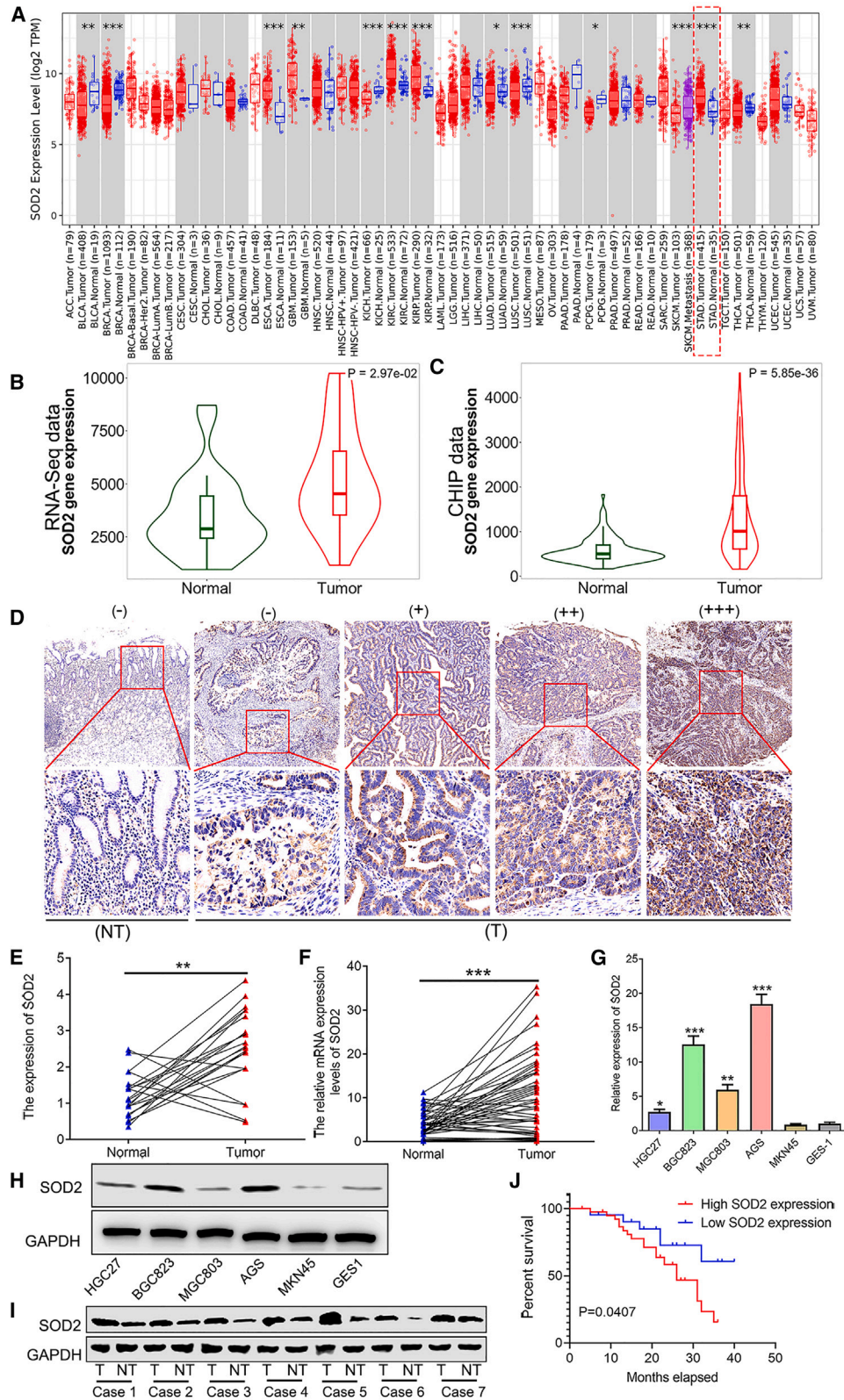
(legend on next page)

metastasis.[14,15] Together, these data suggest an oncogenic function for SOD2 in the pathogenesis and progression of cancer.

H. pylori induces the accumulation of ROS in the human stomach by activating inflammatory pathways,[16] and can also secret virulence factors to induce ROS production and deplete host cells of the antioxidant glutathione (GSH).[17] ROS produced during *H. pylori* infection can promote tumorigenesis; however, the role of SOD2 in GC, correlated with *H. pylori* infection and elevated ROS levels, remains largely unclear. In the present study, we aimed to investigate the biological characteristics and function of SOD2 in response to *H. pylori* infection in GC.

RESULTS

Overexpression of superoxide dismutase is a marker of poor prognosis in gastric cancer

Firstly, to explore the expression of SOD2 in GC, we analyzed the data from the TIMER and TNMplot online databases. The results demonstrated that SOD2 expression levels were significantly higher in GC tissues than in comparable normal tissues (Figures 1A–1C). To examine the SOD2 protein level in GC tissues, IHC was conducted on human paracancerous control tissues ($N = 23$) and GC tissues ($N = 23$). No patients had received preoperative chemotherapy or radiotherapy. Our results indicated that SOD2 protein levels are significantly higher in GC than in the paracancerous samples (Figures 1D and 1E). Subsequently, qRT-PCR data showed that the SOD2 mRNA level was significantly higher in GC tissues ($N = 35$) than in normal control tissues ($N = 35$) (Figure 1F). Moreover, the qRT-PCR and western blot assay results further confirmed that the expression levels of SOD2 were mostly upregulated in GC cell lines compared with GES1 gastric epithelium cells at both mRNA and protein levels (Figures 1G and 1H). However, the levels of SOD2 were different in various GC lines, and low expression of SOD2 in metastatic GC cell lines could be due to the individual genetic background differences. We also found that SOD2 protein levels were clearly increased in fresh GC tissues compared with adjacent normal samples (Figure 1I). In addition, Kaplan–Meier survival analysis demonstrated that patients with GC in our cohort with a higher level of SOD2 had a poorer overall survival rate than those with a lower SOD2 level (Figure 1J). Collectively, these data show that SOD2 is overexpressed in GC and indicates a poor prognosis.

H. pylori promotes superoxide dismutase expression in gastric cancer cells

H. pylori infection is a major risk factor for GC. Therefore, we detected whether SOD2 expression is associated with *H. pylori*

infection in GC. To verify the gene alterations mediated by *H. pylori* infection in GC cells, we conducted RNA-seq to show the gene expression alterations in MGC803 cells co-cultured with or without *H. pylori* for 6 h. After the screening (fold change >2, *p* value <0.05, and FDR <0.05), the gene expression profiles suggested that 179 genes were differentially expressed in *H. pylori*-infected MGC803 cells, including 162 overexpressed genes and 17 downregulated genes (Figures 2A and 2B). SOD2 was upregulated in *H. pylori*-infected MGC803 cells (Figure 2C), and the upregulation of SOD2 in *H. pylori*-infected gastritis epithelium was also supported by comparing the *H. pylori*-positive gastritis samples with *H. pylori*-negative samples from the GEO dataset (GSE60427) (Figure 2D). After culturing MGC803 and AGS cells with the *H. pylori* strains 26695 and 43504, qRT-PCR analysis demonstrated that *H. pylori* infection increased the SOD2 mRNA level (Figures 2E and 2F). To further validate the *in vitro* findings, we applied an *H. pylori* infection mouse model. C57BL/6 mice were gavaged with Brucella broth (control) or *H. pylori* strain PMSS1. qRT-PCR data indicated that infection with PMSS1 led to a significantly higher SOD2 mRNA level than the negative control (Figure 2G). Meanwhile, IHC results demonstrated that SOD2 protein levels were significantly higher in PMSS1-infected mice than in the negative control (Figure 2H). Subsequently, MGC803 and AGS cells were tested to explore whether *H. pylori* infection increased the SOD2 expression level by activating the NF-κB pathway in gastric cells. The activity of SOD2 is strongly influenced by its acetylation status, with the acetylation of SOD2 at the K122 and K68 residues inhibiting its catalytic activity.[18] Western blot assay confirmed that *H. pylori* infection upregulated SOD2 and p-p65 (S536) proteins, validating the activation of the NF-κB pathway (Figures 2I and 2J) and consistent with previous research.[19] Consistent with the *in vitro* results, our findings from C57BL/6 mice gavaged with PMSS1 for 14 days also suggested that *H. pylori* infection could enhance the SOD2 and p-p65 (S536) expression levels (Figure 2K). Furthermore, we observed significant inhibition of SOD2 acetylation at K122 following *H. pylori* infection *in vivo* and *in vitro*, indicating an enhancement in SOD2 antioxidant enzymatic activity (Figures 2I–2K). Therefore, these findings demonstrate that *H. pylori* can promote SOD2 expression as well as increase SOD2 antioxidant enzymatic activity in gastric cells.

NF-κb transcriptionally upregulates superoxide dismutase expression

To further define the regulatory relationship between SOD2 and the NF-κB pathway, we detected whether SOD2 affected NF-κB phosphorylation in MGC803 and AGS cells. Western blot data indicated that the upregulation of SOD2 in MGC803 cells had

---

Figure 1. SOD2 is upregulated in gastric cancer (GC) and predicts a poor prognosis

(A-C) The relative expression levels of SOD2 in GC tissues and comparable normal tissues by analyzing the TIMER and TNMplot online databases.

(D and E) IHC staining of SOD2 in non-cancerous gastric and GC tissues.

(F) Relative expression of SOD2 in 35 GC samples detected by qRT-PCR.

(G) The relative expression levels of SOD2 in GC cell lines compared with GES1 were determined by qRT-PCR in three independent experiments.

(H and I) Western blot assay of SOD2 and GAPDH in GES1, GC cell lines, GC tissues, and comparable normal tissues. GAPDH was used as a loading control.

(J) Kaplan–Meier analysis demonstrates that a high SOD2 level correlated with the overall survival (OS) of patients with GC. Each bar represents the mean ± SD for triplicate experiments; statistical analysis by ANOVA or Student's t test: *$p < 0.05$, **$p < 0.01$, ***$p < 0.001$ versus the indicated group.
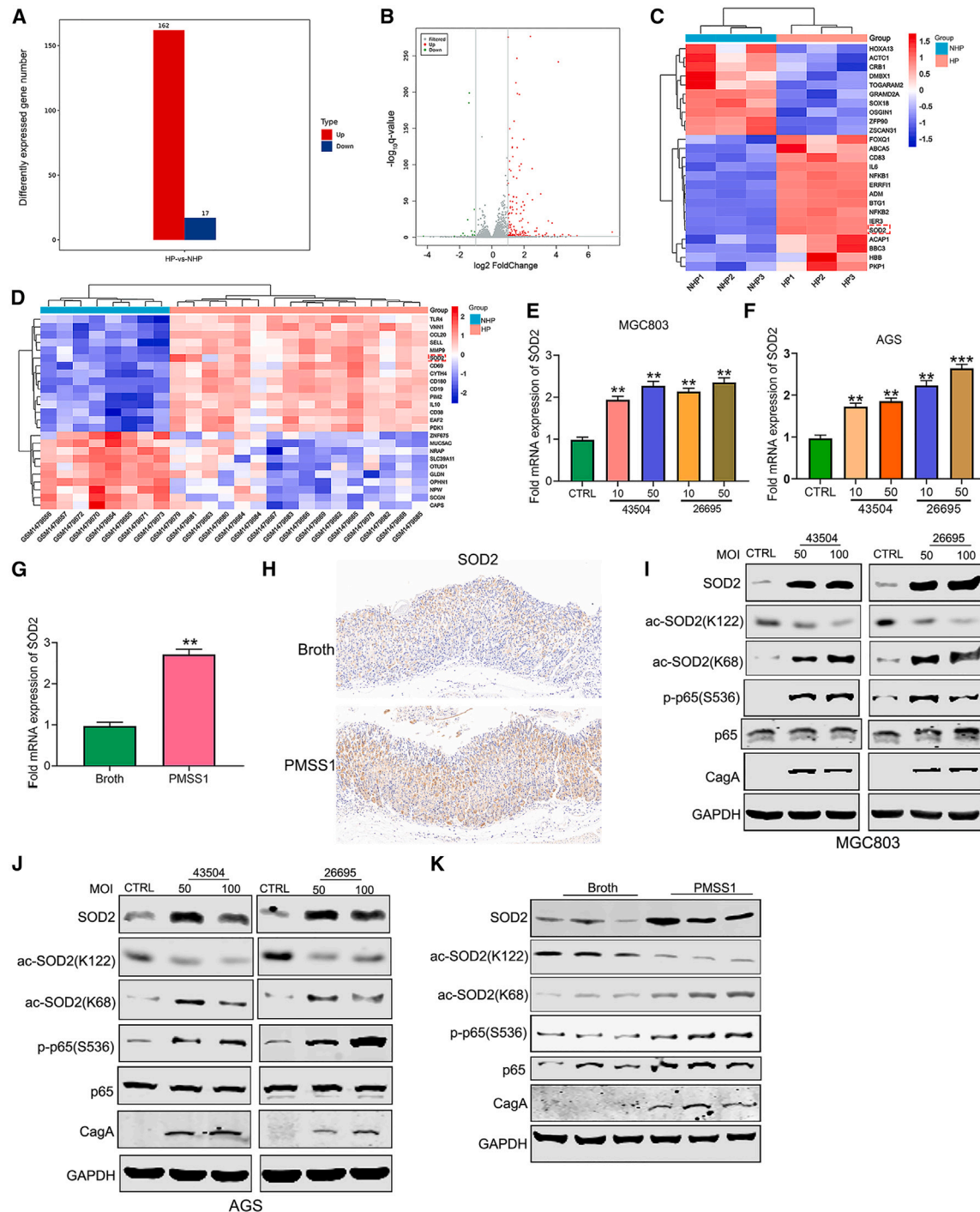
Figure 2. *H. pylori* infection facilitates the SOD2 expression and activation of NF-κB

(A and B) RNA-seq demonstrates that 179 differentially expressed genes were detected in *H. pylori*-infected MGC803 cells, including 162 upregulated genes and 17 downregulated genes.

(C) Heatmap revealing 15 upregulated and 10 downregulated mRNAs in RNA-seq analysis of *H. pylori*-infected MGC803 cells and uninfected negative control cells.

(D) GEO dataset (GSE60427) analyses demonstrate that the SOD2 mRNA level is higher in *H. pylori*-positive gastritis samples than in *H. pylori*-negative gastritis samples.

(E and F) qRT-PCR assay of SOD2 in MGC803 and AGS cells treated with and without *H. pylori* strains (43504 and 26695).

(G) qRT-PCR assay of SOD2 in gastric tissues of mice treated with Brucella broth (control) or PMSS1 for 14 days.

(legend continued on next page)

no obvious impact on p65 and p-p65 (S536) expression (Figure 3A). Downregulation of SOD2 in AGS cells also had no impact on the p65 and p-p65 (S536) expression levels (Figure 3B). More importantly, the NF-κB luciferase reporter results demonstrated that the upregulation of SOD2 in MGC803 cells had no impact on the transcriptional activity of NF-κB in the absence or presence of TNF-α treatment (Figure 3C). Therefore, our data clearly show that SOD2 has no effect on the regulation of NF-κB transcription activity.

To investigate the biological signaling pathways participating in H. pylori-related GC tumorigenesis, we used gene set enrichment analysis (GSEA). GSEA enrichment plots revealed that cancer-related pathways and the TNF and NF-κB signaling pathways were more strongly associated with H. pylori-infected GC cells than controls (Figure 3D). We further explored whether NF-κB regulated SOD2 expression. To determine whether H. pylori infection results in the subsequent activation of the NF-κB pathway, MGC803 cells were infected with H. pylori strain 26695 or 43504 in the absence or presence of transfected p-NF-κB luciferase plasmids. Luciferase analysis showed a statistical promotion of NF-κB transcriptional activity following infection with H. pylori, and this increased activity was reversed by an NF-κB inhibitor (Figure 3E). We treated MGC803 and AGS cells with TNF-α or NF-κB inhibitors to activate or suppress the NF-κB pathway and then assessed the SOD2 expression levels. The qRT-PCR and western blot assays verified the upregulation of SOD2 mRNA (Figure 3F) and protein (Figure 3G) levels in MGC803 cells treated with TNF-α. Moreover, inhibition of NF-κB clearly inhibited the expression levels of SOD2 mRNA (Figure 3H) and protein (Figure 3I) in AGS cells. We also verified these results using the transient transfection of NF-κB into MGC803 cells, which resulted in a significant upregulation of SOD2 mRNA (Figure 3J) and protein levels (Figure 3K). In summary, these findings indicate that the NF-κB pathway plays a critical role in the transcriptional regulation of SOD2.

NF-κb binds to the superoxide dismutase promoter

To fully characterize the action of NF-κB at the SOD2 promoter region, we performed a ChIP assay to determine the key NF-κB binding sites. The separate regions of the putative NF-κB binding sites were shown in Figure 4A. To identify the key binding sites regulated by NF-κB in the SOD2 promoter, we constructed three SOD2 luciferase reporter plasmids, P1, P2, and P3, including clusters A, B, and C, respectively. The luciferase assay showed that the activities of SOD2-P2 and SOD2-P3 were not altered in MGC803 cells transfected with the NF-κB-p65 plasmid. However, the activity of the SOD2-P1 luciferase reporter was significantly enhanced in p65-transfected MGC803 cells (Figure 4B). To further validate the interaction between NF-κB p65 and the SOD2 promoter, MGC803 cells were transfected with the SOD2-P1, SOD2-P2, or SOD2-P3 luciferase

gene plasmids, and subsequently treated with TNF-α or TNF-α in combination with an NF-κB inhibitor. The promoter luciferase activity data demonstrated that the activity of SOD2-P1 luciferase was significantly increased in MGC803 cells treated with TNF-α, and treatment with an NF-κB inhibitor reduced the above effects. However, treatment with TNF-α or an NF-κB inhibitor had no impact on the promoter luciferase reporter activity of SOD2-P2 or SOD2-P3 (Figure 4C). Next, we investigated the SOD2-P1 luciferase activity of GC cells treated with H. pylori. Our observations revealed that H. pylori infection (with either 26695 or 43504) led to a significant enhancement of SOD2-P1 luciferase activity (Figure 4D). We also conducted ChIP in MGC803 cells with or without H. pylori 26695 infection to examine whether H. pylori infection could regulate the transcriptional activity of NF-κB at the SOD2 promoter. The RT-PCR data indicated that the transcriptional activity of NF-κB at the SOD2 promoter was higher with 26695 infection than in the control group, demonstrating that H. pylori infection enhances NF-κB binding activity to SOD2 promoter in the region of Primer 1 but not Primers 2 or 3 (Figure 4E). In this study, we also observed a positive correlation between SOD2 expression levels and p-p65 status in human GC tissues (Figure 4F). These findings strongly indicate that NF-κB p65 promotes SOD2 expression by specifically recognizing a binding site in the SOD2 gene promoter.

H. pylori activates the AKT pathway via superoxide dismutase upregulation

H. pylori has been suggested to regulate the activation of the PI3K/AKT pathway.[19] Consistent with this, GSEA analysis of our data showed that the PI3K/AKT signaling pathway was activated in H. pylori-infected GC cells (Figure 3D). Because we had shown that H. pylori infection enhanced SOD2 expression, we next tested whether SOD2 could induce the activation of the AKT pathway as a response to H. pylori infection. Notably, ectopic overexpression of SOD2 in MGC803 cells using pcDNA-SOD2 promoted GC cell survival in vitro (Figure 5A). Meanwhile, a clone formation assay demonstrated significantly enhanced survival of MGC803 cells overexpressing SOD2 compared with control cells following H. pylori infection (Figure 5A). Similarly, the downregulation of SOD2 by siRNA clearly decreased the cell viability of AGS cells treated with H. pylori (Figure 5B), and silencing of SOD2 significantly inhibited cell clonogenic survival in AGS cells treated with H. pylori (Figure 5C). As expected, western blot analysis demonstrated that SOD2 downregulation reduced the p-AKT (S473) protein level in AGS cells treated with H. pylori (Figure 5D). Moreover, downregulated SOD2 expression significantly inhibited cell survival after H. pylori (26695 or 43504) infection in AGS cells (Figure 5E), while the upregulation of SOD2 significantly promoted cell survival following H. pylori infection in MGC803 cells (Figure 5F).

(H) Immunohistochemistry assay of SOD2 in gastric tissues of mice treated with Brucella broth (control) or PMSS1 for 14 days.

(I and J) Western blot assay revealing p-p65 (S536), p65, CagA, SOD2, acetylated SOD2 lysine 68 (ac-SOD2 K68), and acetylated SOD2 lysine 122 (ac-SOD2 K122) proteins in MGC803 and AGS cells in the presence or absence of H. pylori (43504 and 26695) infection.

(K) Western blot assay showing the p-p65 (S536), p65, CagA, SOD2, acetylated SOD2 lysine 68 (ac-SOD2 K68), and acetylated SOD2 lysine 122 (ac-SOD2 K122) levels in gastric tissues of mice treated with Brucella broth (control) or PMSS1 for 14 days. GAPDH was used as a loading control. MOI, multiplicity of infection. Each bar represents the mean ± SD for triplicate experiments; statistical analysis by ANOVA or Student's t test: **p < 0.01 versus the indicated group.
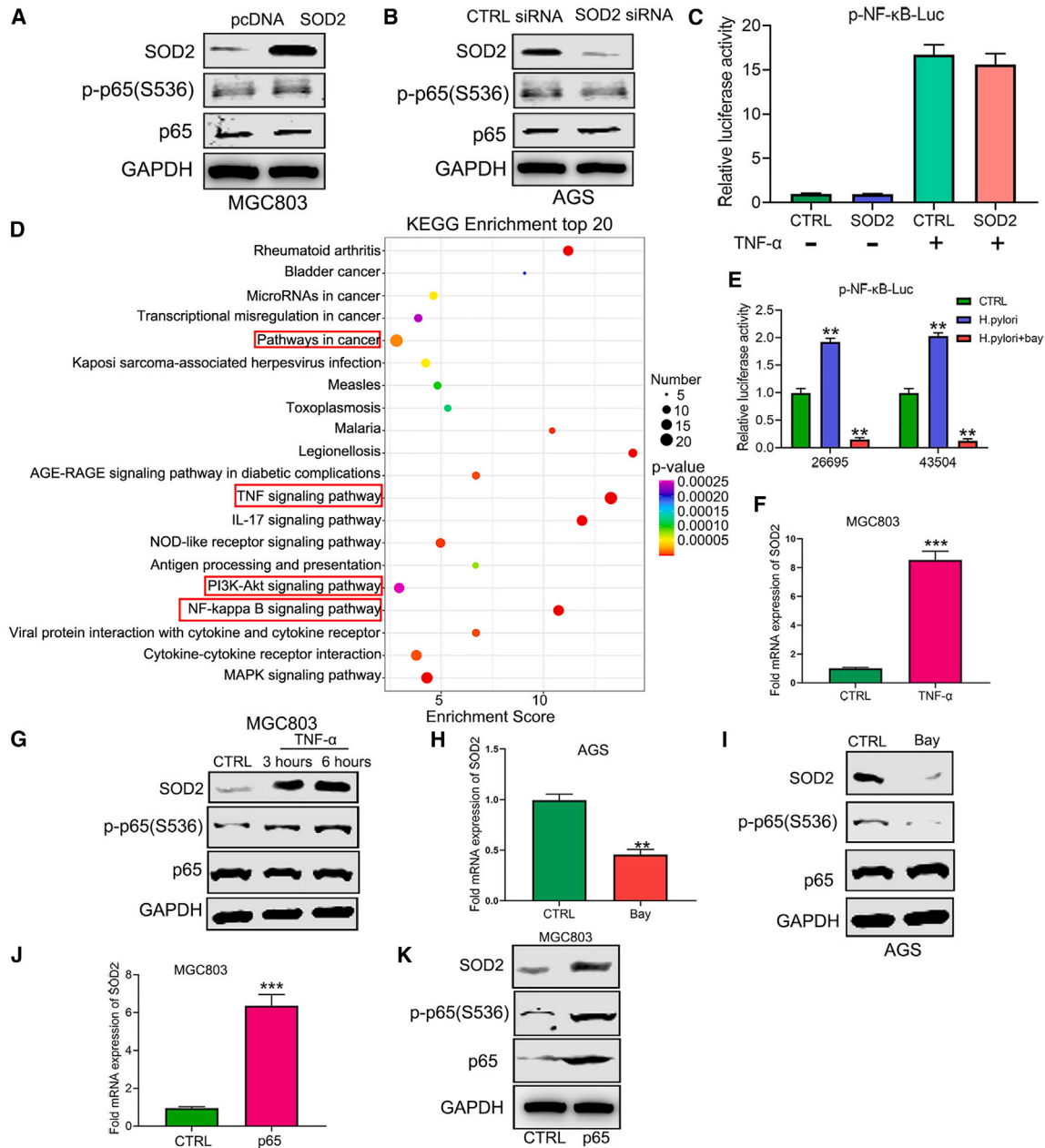
Figure 3. Activation of the NF-κB pathway upregulates SOD2

(A) Western blot assay showing the p-p65 (S536), p65, and SOD2 protein levels in MGC803 cells transfected with SOD2 overexpression plasmids (SOD2) and control plasmids (pcDNA).

(B) Immunoblot assay revealing the p-p65 (S536), p65, and SOD2 protein expression levels in AGS cells transfected with control siRNA and SOD2 siRNA.

(C) Luciferase assay of p-NF-κB-Luc in MGC803 cells overexpressing SOD2 or empty vector in the absence or presence of TNF-α.

(D) KEGG analysis indicates that the DEGs were enriched in biological pathways, including pathways in cancer, the TNF signaling pathway, and the NF-κB signaling pathway.

(E) Luciferase assay of p-NF-κB-Luc in MGC803 cells treated without infection, with *H. pylori* infection, or infection in combination with NF-κB inhibitor Bay 11–7082.

(F and G) qRT-PCR (F) and immunoblot (G) assays of SOD2 were conducted in MGC803 cells treated with TNF-α.

(H and I) qRT-PCR (H) and Western blot (I) assays of SOD2 were conducted in AGS cells treated with NF-κB inhibitor.

(J and K) qRT-PCR (J) and Western blot (K) assays were conducted to detect the SOD2 expression levels in MGC803 cells transfected with p65 plasmids or empty vectors. Each bar represents the mean ± SD for triplicate experiments; statistical analysis by Student's t test: **$p < 0.01$, ***$p < 0.001$ versus the indicated group.
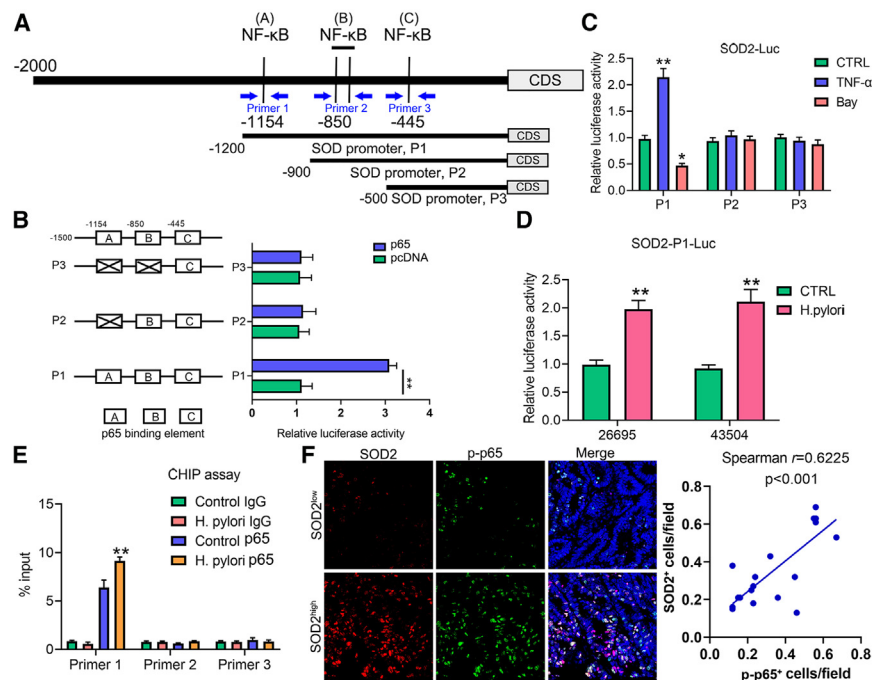
Figure 4. NF-κB binds to the SOD2 promoter region

(A) Diagrammatic sketch of the luciferase reporters revealing the specific DNA sequences within the SOD2 promoter.

(B) Luciferase analysis of the SOD2 promoter luciferase reporter assays in MGC803 cells transfected with NF-kB or pcDNA.

(C) Luciferase assay of the SOD2 promoter luciferase reporters in MGC803 cells treated with TNF-α or NF-κB inhibitor for 3 h.

(D) Luciferase analysis of P1 in MGC803 cells treated with *H. pylori* at 100 MOI for 3 h.

(E) qRT-PCR analysis conducted in MGC803 cells following NF-kB pull down to explore the NF-kB binding sites within the SOD2 promoter.

(F) GC tissues were stained with SOD2 and p-p65 by immunofluorescence staining. Spearman's rank correlation analysis was used to evaluate the correlation of SOD2 and p-p65 expression. Each bar represents the mean ± SD for triplicate experiments; statistical analysis by Student's t test: *$p < 0.05$, **$p < 0.01$ versus the indicated group.

Moreover, the Western blot assay demonstrated that *H. pylori* infection after SOD2 overexpression in MGC803 cells enhanced the *p*-AKT (S473) protein level (Figure 5G). In summary, these findings strongly suggest that *H. pylori* activates the AKT pathway via the upregulation of SOD2.

H. pylori modulates the redox status of gastric cancer cells by upregulating superoxide dismutase/GPX4 expression

SOD2 is localized in mitochondria and scavenges superoxide radicals generated from the respiratory electron transport chain.[9] Therefore, we detected whether SOD2 could modulate the redox status of GC cells infected with *H. pylori*. Our findings indicated that the inhibition of SOD2 expression significantly enhanced the superoxide level in AGS cells following *H. pylori* (strain 26695 or 43504) infection (Figure 6A), while the upregulation of SOD2 significantly reduced the superoxide level after infection with *H. pylori* (26695 or 43504) in MGC803 cells (Figure 6B). These results are consistent with previous studies.[20,21] MDA and 4-HNE are widely used as lipid peroxidation products.[22] Measurement of the MDA and 4-HNE levels represents the degree of oxidative stress and can be used to monitor the redox status. We explored whether SOD2 could regulate the MDA and 4-HNE levels following *H. pylori* infection. The results suggested that SOD2 knockdown significantly increased the MDA and 4-HNE levels in AGS cells following *H. pylori* (26695 or 43504) infection (Figures 6C and 6E), while SOD2 upregulation reduced MDA and 4-HNE levels in MGC803 cells after infection with either *H. pylori* strain (26695 or 43504) (Figures 6D and 6F). Mitochondrial redox homeostasis can be regulated by activating the SIRT3–SOD2–GPX4 signaling pathway.[23] As expected, the GPX4 protein levels were enhanced in AGS cells infected with *H. pylori* 26695 (Figures 6G and 6H).

We then investigated the upstream regulators of *H. pylori*-modulated GPX4 expression. Our findings revealed no statistical difference in GPX4 mRNA levels following *H. pylori* 26695 infections at different time points and MOI (Figures 6I and 6J). We speculated that *H. pylori* possibly increased GPX4 expression levels by enhancing GPX4 stability. To ascertain whether *H. pylori* can promote GPX4 protein stability, we analyzed GPX4 degradation following treatment with cycloheximide (CHX). The results showed that *H. pylori* significantly reduced the degradation of GPX4 (Figure 6K). Moreover, our data showed that the AKT inhibitor MK2206 significantly down-regulated GPX4 protein levels in GC cells infected with *H. pylori* (Figure 6L). It has been reported that GPX4 could be degraded by chaperone-mediated autophagy.[24] We found that chaperone HSC70 knockdown elevated the protein levels of GPX4 (Figure 6M). More importantly, our data further confirmed that *H. pylori* inhibited the binding of GPX4 to HSC70 in GC cells, while MK2206 reversed the *H. pylori*-induced decrease in the binding of GPX4 to HSC70 (Figure 6N). These results demonstrate that AKT can inhibit the autophagic degradation to enhance the stability of GPX4. Taken together, we conclude that AKT-mediated decrease of GPX4 degradation accounts for the enhanced GPX4 expression levels in GC cells treated with *H. pylori*.

Superoxide dismutase inhibits ferroptosis in gastric cancer cells

SOD2 is involved in the regulation of ROS detoxification. Ferroptosis is a specific cell death induced by the additional accumulation of lipid ROS and is involved in the development of various types of tumors.[25] We next investigated whether SOD2 regulated ferroptosis. We detected the impact of SOD2 on ferroptosis and clarified that SOD2 inhibition promoted erastin-induced ferroptosis (Figure 7A). This effect was reversed by treatment with the ferroptosis
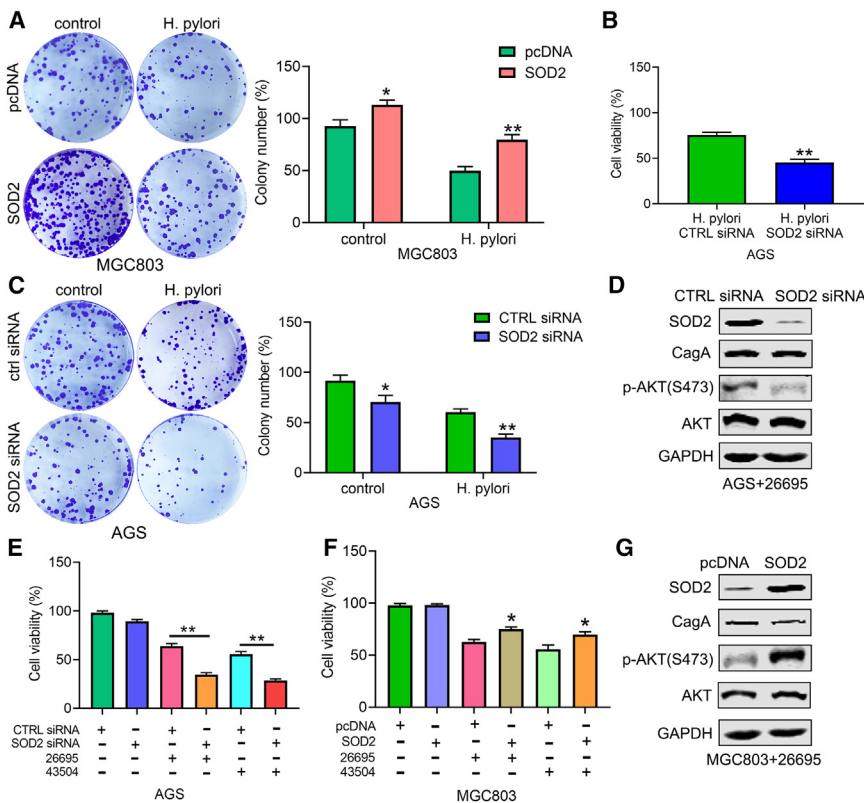
Figure 5. *H. pylori* promotes AKT activation via the regulation of SOD2

(A) Clonogenic assay showing a clear increase of colony number in MGC803 cells expressing SOD2 after *H. pylori* infection.

(B) The cell viability was significantly reduced by the downregulation of SOD2 in AGS cells treated with *H. pylori* infection.

(C) Clonogenic assay demonstrating that the silencing of SOD2 significantly decreased the number of colonies in AGS treated with *H. pylori* infection.

(D) Western blot assay showing the SOD2, AKT, *p*-AKT (S473), and CagA proteins in AGS cells infected with *H. pylori* and transfected with SOD2 siRNA or control siRNA.

(E) The downregulation of SOD2 in AGS cells results in the significant inhibition of cell survival in *H. pylori* infection.

(F) Upregulation of SOD2 in MGC803 cells significantly increases cell survival after *H. pylori* infection.

(G) Western blot assay shows the SOD2, AKT, *p*-AKT (S473), and CagA protein levels in MGC803 cells infected with *H. pylori* and transfected with SOD2 overexpression plasmids (SOD2) and control plasmids (pcDNA). Each bar represents the mean ± SD for triplicate experiments; statistical analysis by Student's t test: *$p < 0.05$, **$p < 0.01$ versus the indicated group.

inhibitor ferrostatin-1 (Figures 7B and 7C). Meanwhile, SOD2 overexpression in GC cells caused strong resistance to erastin-induced ferroptosis (Figure 7D). GSH, an important intracellular antioxidant, can inhibit ferroptosis by eliminating lipid hydrogen peroxide. We found that the downregulation of SOD2 significantly decreased the GSH level in AGS cells after erastin treatment, and this effect was reversed by treatment with the ferroptosis inhibitor ferrostatin-1 (Figure 7E). SOD2 overexpression further promoted the GSH level in MGC803 cells after treatment with erastin, which was also rescued by treatment with ferrostatin-1 (Figure 7F). Ferroptosis can be attenuated in diabetic nephropathy by activating the SIRT3–SOD2–GPX4 signaling pathway. GPX4 is the key regulator of ferroptosis by scavenging lipid hydroperoxides.[26] Western blot data reconfirmed that interference with SOD2 expression clearly inhibited GPX4 expression, while the upregulation of SOD2 enhanced GPX4 expression (Figure 7G). Our data showed poor survival in patients with high levels of SOD2. 5-FU is generally used as a first-line treatment for GC,[27] and leads to a cytotoxic effect by enhancing ROS generation.[28] We found that SOD2 inhibited ferroptosis by regulating the intracellular levels of GSH. We also confirmed that the downregulation of SOD2 increased the chemosensitivity of AGS and MGC803 cells to 5-FU treatment. The IC50 of 5-FU decreased from 3.620 μM to 2.306 μM following SOD2 knockdown in AGS cells (Figure 7H). Similar findings were also observed in MGC803 cancer cells (Figure 7I). The results demonstrated that patients with GC in the TCGA cohort with a higher level of GPX4 had a poorer overall survival rate compared with those with a lower GPX4 level (Figure 7J). We also performed

western blot analysis for SOD2 in surgically resected GC samples from patients receiving 5-FU-based chemotherapy. The results showed that patients 11 and 12 were chemotherapy resistant, while patient 13 was sensitive to chemotherapy (Figure 7K). To further explore the role of SOD2 on tumor growth and 5-FU sensitivity *in vivo*, we injected SOD2 knockdown and control MGC803 cells into the nude mice and analyzed the tumorigenesis. Compared with the control cells, the knockdown of SOD2 greatly repressed tumor growth and enhanced 5-FU sensitivity (Figure 7L). In summary, these data collectively suggest that SOD2 acts as a repressor of ferroptosis and enhances resistance to 5-FU in GC.

DISCUSSION

Overexpression of SOD2 is frequently observed in human cancers.[12,29] Although a high level of SOD2 has been associated with GC,[30] the potential molecular mechanisms have not been fully elucidated. *H. pylori* infection has been widely acknowledged as the major risk factor for GC.[31] The purpose of the current study was to explore whether *H. pylori* infection could promote SOD2 expression, further facilitating gastric carcinogenesis. As expected, *H. pylori* infection enhanced SOD2 expression, supporting the hypothesis that SOD2 plays functional roles in *H. pylori*-mediated gastric carcinogenesis. The initiation of the NF-κB pathway by *H. pylori* infection has been the focus of many studies because of its vital function in the regulation of inflammation. Our results reveal that *H. pylori* infection stimulates the NF-κB pathway, promoting the transcriptional upregulation of SOD2;
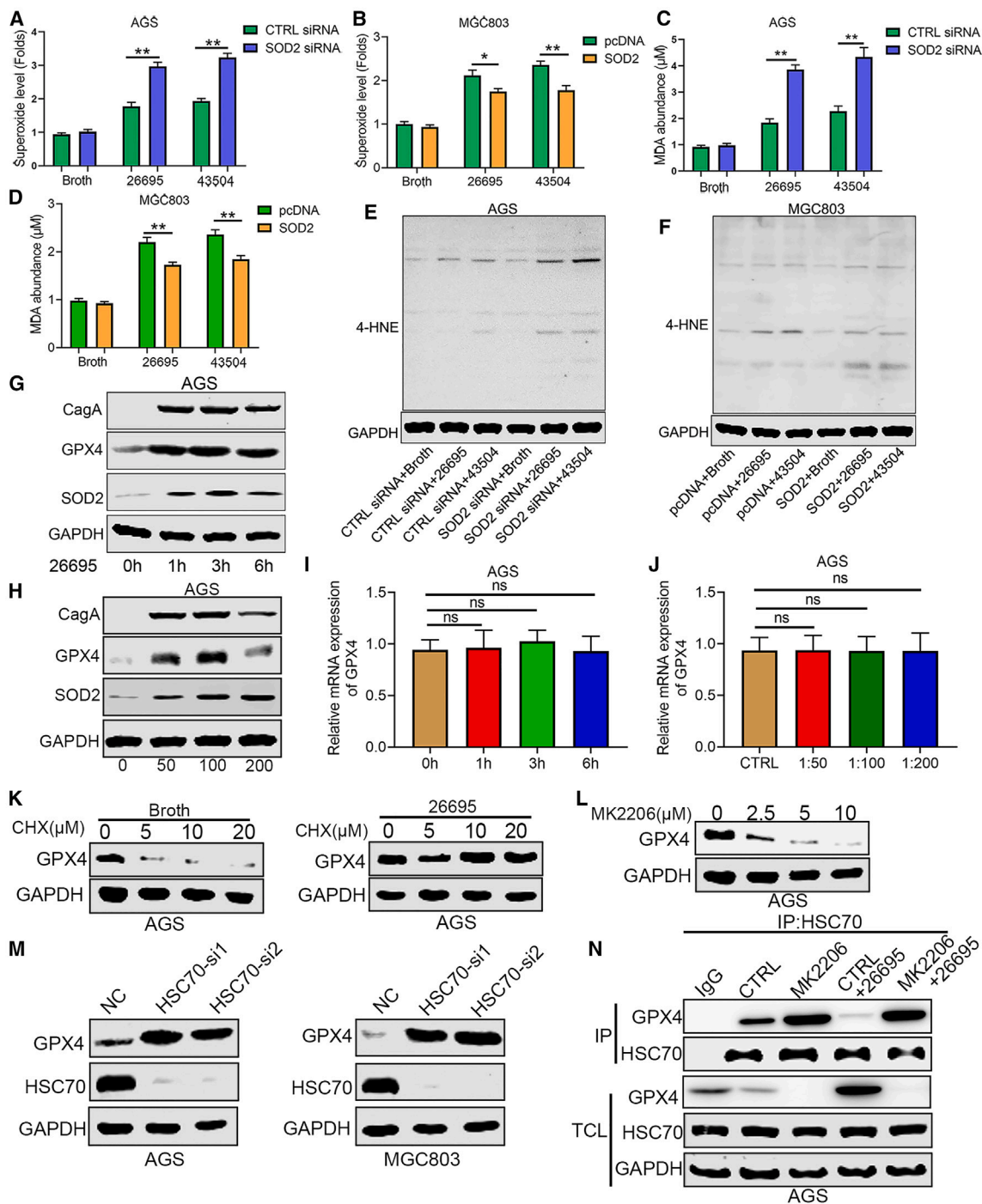
Figure 6. *H. pylori* modulates the redox status of GC cells by upregulating SOD2/GPX4 expression

(A) Levels of superoxide in AGS cells infected with *H. pylori* and transfected with SOD2 siRNA or control siRNA.

(B) Levels of superoxide in MGC803 cells infected with *H. pylori* and transfected with SOD2 overexpression plasmids (SOD2) and control plasmids (pcDNA).

(C) Levels of MDA abundance in AGS cells treated with *H. pylori* and transfected with SOD2 siRNA or control siRNA, reflecting the degree of oxidative stress.

(D) Levels of MDA abundance in MGC803 cells after *H. pylori* infection and transfection with SOD2 overexpression plasmids (SOD2) and control plasmids (pcDNA). (E) Levels of 4-HNE abundance in AGS treated with *H. pylori* and transfected with SOD2 siRNA or control siRNA, another indication of the degree of oxidative stress.

(F) Levels of 4-HNE abundance in MGC803 cells infected with *H. pylori* and transfected with SOD2 overexpression plasmids (SOD2) and control plasmids (pcDNA).

(G and H) Western blot assay revealing the CagA, GPX4, and SOD2 proteins in AGS cells infected with *H. pylori* 26695 at different time points (G) and MOI (H).

(I and J) qRT-PCR assay showing the GPX4 mRNA levels in AGS cells following *H. pylori* 26695 infection at different time points (I) and MOI (J).

(K) An immunoblot shows the expression of GPX4 in AGS cells treatment with control or *H. pylori* 26695 with or without CHX.

(legend continued on next page)

this further activates the AKT signaling pathway involved in gastric tumorigenesis. In addition, SOD2 can serve as an inhibitor of ferroptosis, enhancing resistance to 5-FU in GC cells (Figure 8).

To confirm the molecular alterations regulated by *H. pylori* infection in GC cells, we employed RNA-seq to characterize the gene expression profiles of MGC803 cells co-cultured in the absence or presence of *H. pylori*. Following bioinformatics analysis and a literature review, SOD2 was identified as the target gene in the current study. Upregulation of SOD2 in *H. pylori*-infected gastritis was also confirmed by analyzing a GEO dataset (GSE60427). Together, these results suggest that SOD2 upregulation mediated by *H. pylori* infection facilitates the development of GC.

SOD2 expression can be regulated by a series of inflammatory cytokines and redox activators via transcriptional and post-transcriptional regulatory mechanisms.[32] Activation of the NF-κB pathway is a key regulator of inflammation-related tumor progression, and *H. pylori* infection is thought to generate an inflammatory microenvironment by activating the NF-κB pathway.[33] Our findings revealed the transcriptional upregulation of SOD2 by NF-κB during *H. pylori* infection and confirmed crucial NF-κB binding sites in the SOD2 promoter. Meanwhile, the luciferase results were confirmed by ChIP assay. Thus, we have revealed a new molecular mechanism upregulating SOD2 expression in GC cells that is strongly correlated with *H. pylori*-induced inflammation.

When the homeostasis between ROS generation and elimination is destroyed, the additional ROS agents lead to oxidative stress. During tumorigenesis, intrinsic oxidative stress is thought to play significant roles not only in cell proliferation and genetic instability but also in the evasion of cell death.[34,35] Superoxide radicals can be degraded by the mitochondrial antioxidase SOD2, producing H_2O_2 and molecular oxygen. Anticancer drugs generate excessive ROS, consequently leading to cell death. Suppressing SIRT3 increases the levels of mitochondrial reactive oxygen species (mtROS) by regulating SOD2, and inhibiting SOD2 promotes sensitivity to anticancer drugs in colorectal cancer.[36] SOD2 upregulation results in a stable supply of mitochondrial-derived H_2O_2 that maintains AMPK activation and metabolic alterations, leading to more aggressive breast cancer phenotypes.[37] *H. pylori* infection can increase the amount of ROS and induce oxidative stress.[38,39] On the basis of these findings, gastric epithelial cells are highly likely to generate adaptive mechanisms to protect against *H. pylori*-mediated inflammatory damage. As expected, we detect that *H. pylori* promotes SOD2 expression, and SOD2 is involved in the redox status regulation of GC cells treated with *H. pylori*, promoting gastric cell survival.

Ferroptosis is a specific form of lipid peroxidation-mediated cell death that participates in carcinogenesis, and suppression of ferroptosis has been suggested to promote cancer invasion and metastasis.[40,41] SOD2 is the main antioxidase for superoxide detoxification in mitochondria and is involved in the regulation of the cellular redox status. In this context, we hypothesized that

SOD2 could regulate ferroptosis by affecting the redox status. Therefore, we inhibited the expression of SOD2 in GC cells, which eliminated the protective function of SOD2 on intracellular oxidative stress. Our data suggest that the *H. pylori*-mediated upregulation of SOD2 protects gastric epithelial cells against *H. pylori*-mediated inflammatory damage, improving cell survival during *H. pylori* infection. Induction of ferroptosis facilitates chemosensitization and enhances sensitivity to 5-FU.[42] Our data indicate that SOD2 overexpression inhibits ferroptosis, improving cancer cell resistance to 5-FU. Our findings may potentially explain the association between SOD2 upregulation and poor clinical prognosis. Therefore, this study also reveals that SOD2 may be a key mediator of chemotherapy resistance in GC.

In this study, we have demonstrated that the *H. pylori*-induced activation of NF-κB transcriptionally upregulates SOD2 in GC. Our findings provide strong evidence that the upregulation of SOD2 is crucial for supporting GC cell survival and diminishing the enhanced ROS accumulation, resulting from *H. pylori* infection in gastric epithelial cells. A high SOD2 level indicates a poor prognosis in GC that is associated with resistance to 5-FU by inhibiting ferroptosis. SOD2 may therefore be a promising therapeutic target for the treatment of GC. Thus, the *H. pylori*–NF-κB–SOD2–GPX4 axis is a novel carcinogenic mechanism in gastric tumorigenesis.

Limitations of the study

Our findings suggest that SOD2 may serve as a promising therapeutic target for GC treatment. However, drugs that directly target SOD2 were not used in this study. In addition, it remains unclear how *H. pylori* specifically activates the NF-κB pathway. Finally, we explored the AKT/GPX4 pathway downstream of SOD2, but further experiments are needed to clarify the underlying regulatory mechanism of SOD2 in GC.

RESOURCE AVAILABILITY

Lead contact
Further information and requests for resources and reagents should be directed to and will be fulfilled by the lead contact, Dr. Weijun Wang (wweijun2023@163.com).

Material availability
This study did not generate new unique reagents.

Data and code availability
- RNA-sequencing data that support the findings of this study have been deposited into the Gene Expression Omnibus (GEO) (https://www.ncbi.nlm.nih.gov/geo/query/acc.cgi?acc=GSE278591). All the data presented in this study will be shared upon reasonable request by the lead contact, Dr. Weijun Wang (wweijun2023@163.com).
- This article does not report any original code.
- Additional information required to reanalyze the data reported in this article is available from the lead contact upon request.

(L) An immunoblot showing the expression of GPX4 in *H. pylori* 26695-treated AGS cells treatment with MK2206 at different concentrations.

(M) An immunoblot shows the expression of GPX4 and HSC70 in AGS and MGC803 cells transfected with negative control (NC) or HSC70 siRNAs.

(N) Endogenous HSC70 was immunoprecipitated from AGS cells subjected to the indicated treatments for 12 h, followed by immunoblotting using antibodies to GPX4 and HSC70. Data are representative of $n = 3$ biologically independent experiments. Each bar represents the mean ± SD; statistical analysis by Student's t test: *$p < 0.05$, **$p < 0.01$, ***$p < 0.001$ versus the indicated group, ns means no significance.
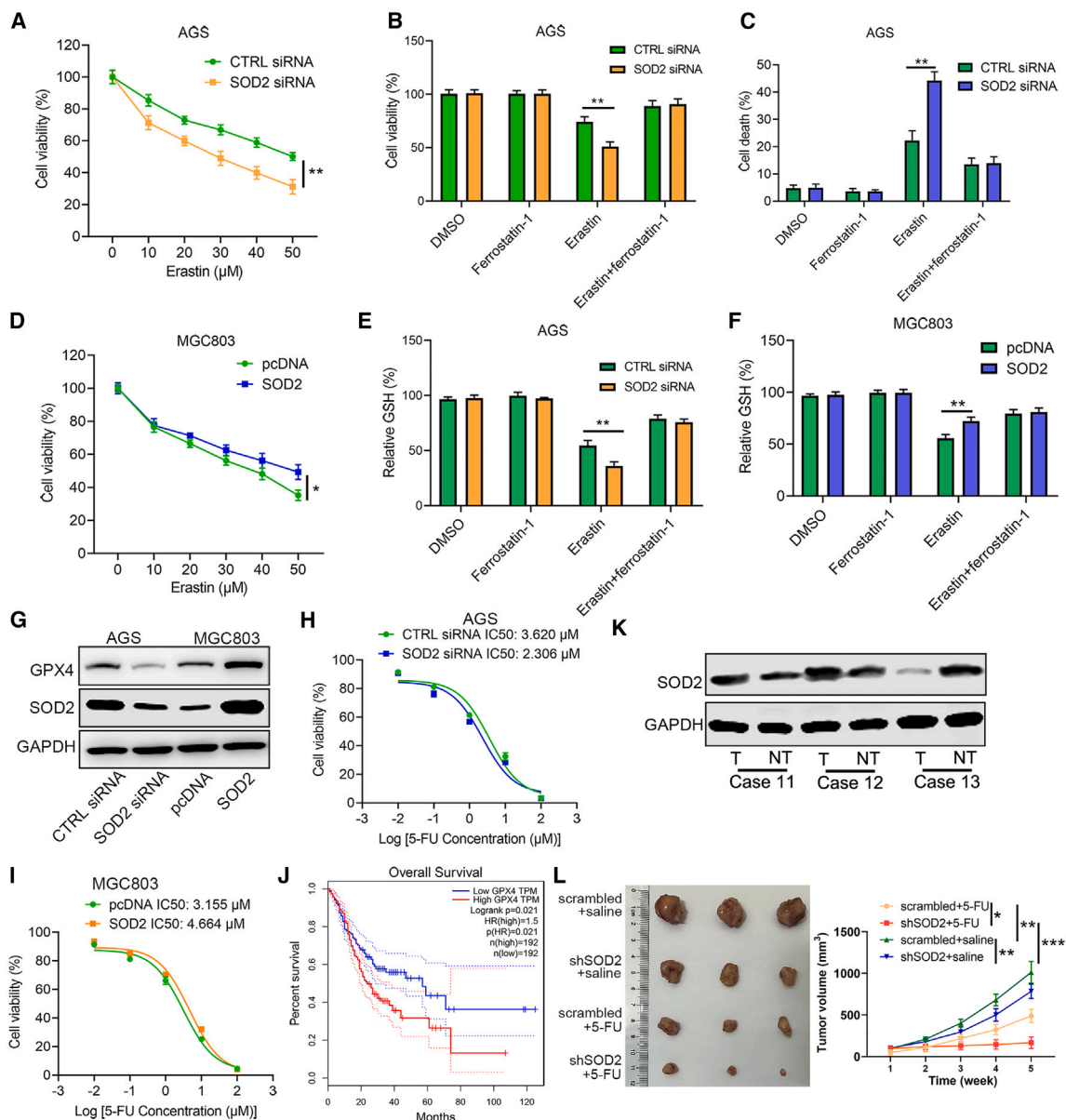
Figure 7. SOD2 acts as an inhibitor of ferroptosis in GC cells

(A) Cell viability of AGS cells transfected with CTRL or SOD2 siRNA following treatment with different concentrations of erastin for 24 h.

(B) Cell viability assay showing AGS cells expressing CTRL or SOD2 siRNA treated with erastin (20 μM) with or without ferrostatin-1 (2 μM) for 24 h.

(C) Cell death assay shows AGS cells transfected with CTRL or SOD2 siRNA after treatment with erastin (20 μM) with or without ferrostatin-1 (2 μM) for 24 h.

(D) Cell viability assay shows MGC803 cells transfected with pcDNA or SOD2 following treatment with different concentrations of erastin for 24 h.

(E) Levels of GSH in control siRNA and SOD2 siRNA AGS cells treated with erastin (20 μM) with or without ferrostatin-1 (2 μM) for 24 h.

(F) Levels of GSH in pcDNA and SOD2 MGC803 cells treated with erastin (20 μM) in the presence or absence of ferrostatin-1 (2 μM) for 24 h.

(G) The expression of GPX4 in AGS and MGC803 cells transfected with SOD2 siRNA or SOD2 overexpression plasmids (SOD2).

(H and I) The 5-FU IC50 was calculated in AGS (H) and MGC803 cells (I).

(J) Kaplan–Meier analysis demonstrates that a high level of GPX4 correlated with a poorer overall survival (OS) of patients with GC in the TCGA dataset.

(K) Western blot assay of SOD2 and GAPDH in GC tissues and comparable normal tissues. GAPDH was used as a loading control.

(L) Photographs of tumors in mice from indicated treatment groups; tumor growth curves demonstrate the development of GC xenografts in nude mice treated with saline and 5-FU. Each bar represents the mean ± SD for triplicate experiments; statistical analysis by Student's t test or two-way ANOVA: *$p < 0.05$, **$p < 0.01$, ***$p < 0.001$ versus the indicated group.
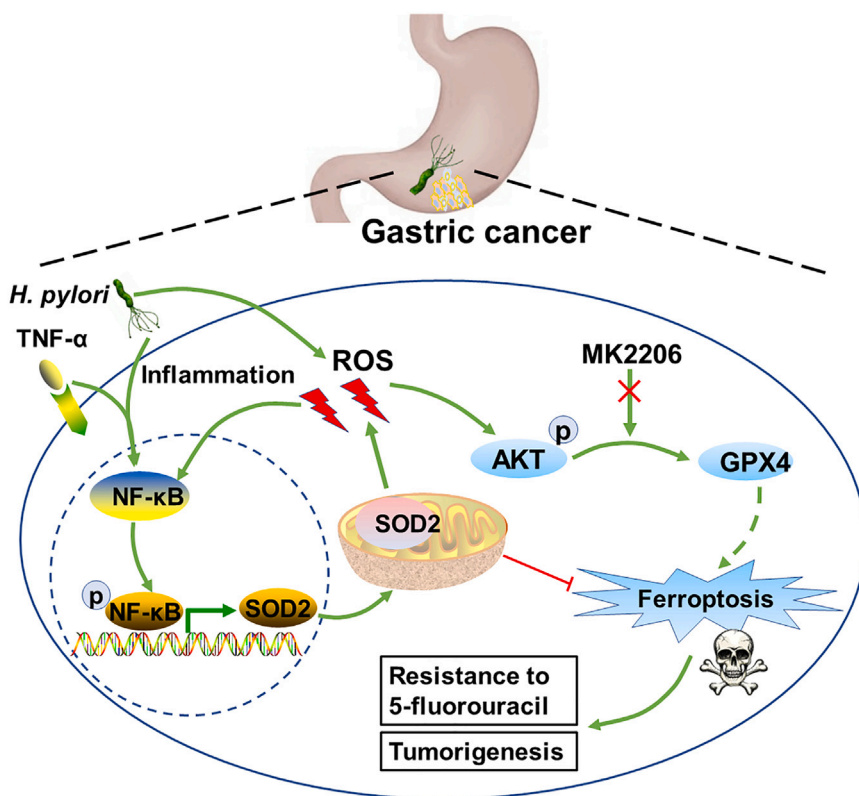
Figure 8. A proposed working model of how the *H. pylori* infection-induced NF-kB signaling pathway upregulates SOD2, leading to the activation of the AKT signaling pathway involved in gastric tumorigenesis, as well as insensitivity to ferroptosis signaling contributing to resistance to 5-FU in GC cells.

AUTHOR CONTRIBUTIONS

H.F., Y.Z., and Y.D. made equal contributions to this research. H.F., Y.Z., X.Z., R.Y., and W.W. conceived and designed the study. H.F., Y.Z., Y.D., J.Y., Z.W., and Z.Z. conducted the experiments, J.X., D.Y., Z.H., and Q.Y. performed data analysis. H.F. and Y.Z. wrote the article. All authors read and approved the final article.

DECLARATION OF INTERESTS

The authors declare no competing interests.

STAR★METHODS

Detailed methods are provided in the online version of this paper and include the following:

- KEY RESOURCES TABLE
- EXPERIMENTAL MODEL AND STUDY PARTICIPANT DETAILS
  - Mouse models
  - Cell culture and reagents
- METHOD DETAILS
  - Patient samples and ethical statement
  - Immunohistochemistry (IHC) and immunofluorescence
  - *H. pylori* culture and infection
  - RNA sequencing analysis (RNA-seq)
  - RNA interference, plasmid construction, and transfection
  - Western blot and immunoprecipitation
  - Quantitative real-time PCR
  - Cell viability assay
  - Superoxide assay
  - ROS assay
  - Lipid peroxidation assay
  - Luciferase reporter assay
  - Chromatin immunoprecipitation assay
  - Colony formation
- QUANTIFICATION AND STATISTICAL ANALYSIS

SUPPLEMENTAL INFORMATION

Supplemental information can be found online at https://doi.org/10.1016/j.isci.2024.111553.

REFERENCES

1. Sung, H., Ferlay, J., Siegel, R.L., Laversanne, M., Soerjomataram, I., Jemal, A., and Bray, F. (2021). Global Cancer Statistics 2020: GLOBOCAN

Estimates of Incidence and Mortality Worldwide for 36 Cancers in 185 Countries. CA A Cancer J. Clin. *71*, 209–249.

2. Polk, D.B., and Peek, R.M., Jr. (2010). Helicobacter pylori: gastric cancer and beyond. Nat. Rev. Cancer. *10*, 403–414.

3. Kumar, S., Metz, D.C., Ellenberg, S., Kaplan, D.E., and Goldberg, D.S. (2020). Risk Factors and Incidence of Gastric Cancer After Detection of Helicobacter pylori Infection: A Large Cohort Study. Gastroenterology *158*, 527–536.

4. Waskito, L.A., Salama, N.R., and Yamaoka, Y. (2018). Pathogenesis of Helicobacter pylori infection. Helicobacter *23*, e12516.

5. Gobert, A.P., and Wilson, K.T. (2017). Polyamine- and NADPH-dependent generation of ROS during Helicobacter pylori infection: A blessing in disguise. Free Radic. Biol. Med. *105*, 16–27.

6. Costa, L., Corre, S., Michel, V., Le Luel, K., Fernandes, J., Ziveri, J., Jouvion, G., Danckaert, A., Mouchet, N., Da Silva Barreira, D., et al. (2020). USF1 defect drives p53 degradation during Helicobacter pylori infection and accelerates gastric carcinogenesis. Gut *69*, 1582–1591.

7. Bolduc, J.A., Collins, J.A., and Loeser, R.F. (2019). Reactive oxygen species, aging and articular cartilage homeostasis. Free Radic. Biol. Med. *132*, 73–82.

8. Chen, C., Zhou, Y., Hu, C., Wang, Y., Yan, Z., Li, Z., and Wu, R. (2019). Mitochondria and oxidative stress in ovarian endometriosis. Free Radic. Biol. Med. *136*, 22–34.

9. Miar, A., Hevia, D., Muñoz-Cimadevilla, H., Astudillo, A., Velasco, J., Sainz, R.M., and Mayo, J.C. (2015). Manganese superoxide dismutase (SOD2/MnSOD)/catalase and SOD2/GPx1 ratios as biomarkers for tumor progression and metastasis in prostate, colon, and lung cancer. Free Radic. Biol. Med. *85*, 45–55.

10. Weydert, C., Roling, B., Liu, J., Hinkhouse, M.M., Ritchie, J.M., Oberley, L.W., and Cullen, J.J. (2003). Suppression of the malignant phenotype in human pancreatic cancer cells by the overexpression of manganese superoxide dismutase. Mol. Cancer Therapeut. *2*, 361–369.

11. Huang, Y., He, T., and Domann, F.E. (1999). Decreased expression of manganese superoxide dismutase in transformed cells is associated with increased cytosine methylation of the SOD2 gene. DNA. Cell. Biol. *18*, 643–652.

12. Hemachandra, L.P.M.P., Shin, D.H., Dier, U., Iuliano, J.N., Engelberth, S.A., Uusitalo, L.M., Murphy, S.K., and Hempel, N. (2015). Mitochondrial Superoxide Dismutase Has a Protumorigenic Role in Ovarian Clear Cell Carcinoma. Cancer. Res. *75*, 4973–4984.

13. Alateyah, N., Gupta, I., Rusyniak, R.S., and Ouhtit, A. (2022). SOD2, a Potential Transcriptional Target Underpinning CD44-Promoted Breast Cancer Progression. Molecules *27*, 811.

14. Nelson, K.K., Ranganathan, A.C., Mansouri, J., Rodriguez, A.M., Providence, K.M., Rutter, J.L., Pumiglia, K., Bennett, J.A., and Melendez, J.A. (2003). Elevated sod2 activity augments matrix metalloproteinase expression: evidence for the involvement of endogenous hydrogen peroxide in regulating metastasis. Clin. Cancer. Res. *9*, 424–432.

15. Nelson, K.K., Subbaram, S., Connor, K.M., Dasgupta, J., Ha, X.F., Meng, T.C., Tonks, N.K., and Melendez, J.A. (2006). Redox-dependent matrix metalloproteinase-1 expression is regulated by JNK through Ets and AP-1 promoter motifs. J. Biol. Chem. *281*, 14100–14110.

16. Davies, G.R., Simmonds, N.J., Stevens, T.R., Sheaff, M.T., Banatvala, N., Laurenson, I.F., Blake, D.R., and Rampton, D.S. (1994). Helicobacter pylori stimulates antral mucosal reactive oxygen metabolite production in vivo. Gut *35*, 179–185.

17. Hardbower, D.M., de Sablet, T., Chaturvedi, R., and Wilson, K.T. (2013). Chronic inflammation and oxidative stress: the smoking gun for Helicobacter pylori-induced gastric cancer? Gut Microb. *4*, 475–481.

18. Martell, E., Kuzmychova, H., Kaul, E., Senthil, H., Chowdhury, S.R., Morrison, L.C., Fresnoza, A., Zagozewski, J., Venugopal, C., Anderson, C.M., et al. (2023). Metabolism-based targeting of MYC via MPC-SOD2 axis-mediated oxidation promotes cellular differentiation in group 3 medulloblastoma. Nat. Commun. *14*, 2502.

19. Cao, L., Zhu, S., Lu, H., Soutto, M., Bhat, N., Chen, Z., Peng, D., Lin, J., Lu, J., Li, P., et al. (2022). Helicobacter pylori-induced RASAL2 Through Activation of Nuclear Factor-κB Promotes Gastric Tumorigenesis via β-catenin Signaling Axis. Gastroenterology *162*, 1716–1731.e17.

20. Pi, H., Xu, S., Reiter, R.J., Guo, P., Zhang, L., Li, Y., Li, M., Cao, Z., Tian, L., Xie, J., et al. (2015). SIRT3-SOD2-mROS-dependent autophagy in cadmium-induced hepatotoxicity and salvage by melatonin. Autophagy *11*, 1037–1051.

21. Ren, T., Zhang, H., Wang, J., Zhu, J., Jin, M., Wu, Y., Guo, X., Ji, L., Huang, Q., Zhang, H., et al. (2017). MCU-dependent mitochondrial Ca(2+) inhibits NAD(+)/SIRT3/SOD2 pathway to promote ROS production and metastasis of HCC cells. Oncogene *36*, 5897–5909.

22. Tsikas, D. (2017). Assessment of lipid peroxidation by measuring malondialdehyde (MDA) and relatives in biological samples: Analytical and biological challenges. Anal. Biochem. *524*, 13–30.

23. Li, Q., Liao, J., Chen, W., Zhang, K., Li, H., Ma, F., Zhang, H., Han, Q., Guo, J., Li, Y., et al. (2022). NAC alleviative ferroptosis in diabetic nephropathy via maintaining mitochondrial redox homeostasis through activating SIRT3-SOD2/Gpx4 pathway. Free. Radic. Biol. Med. *187*, 158–170.

24. Xie, Y., Kang, R., Klionsky, D.J., and Tang, D. (2023). GPX4 in cell death, autophagy, and disease. Autophagy *19*, 2621–2638.

25. Chen, X., Kang, R., Kroemer, G., and Tang, D. (2021). Broadening horizons: the role of ferroptosis in cancer. Nat. Rev. Clin. Oncol. *18*, 280–296.

26. Hassannia, B., Vandenabeele, P., and Vanden Berghe, T. (2019). Targeting Ferroptosis to Iron Out Cancer. Cancer. Cell. *35*, 830–849.

27. Smyth, E.C., Nilsson, M., Grabsch, H.I., van Grieken, N.C., and Lordick, F. (2020). Gastric cancer. Lancet *396*, 635–648.

28. Longley, D.B., Harkin, D.P., and Johnston, P.G. (2003). 5-fluorouracil: mechanisms of action and clinical strategies. Nat. Rev. Cancer *3*, 330–338.

29. Ye, H., Wang, A., Lee, B.S., Yu, T., Sheng, S., Peng, T., Hu, S., Crowe, D.L., and Zhou, X. (2008). Proteomic based identification of manganese superoxide dismutase 2 (SOD2) as a metastasis marker for oral squamous cell carcinoma. Cancer Genomics Proteomics *5*, 85–94.

30. Janssen, A.M., Bosman, C.B., van Duijn, W., Oostendorp-van de Ruit, M.M., Kubben, F.J., Griffioen, G., Lamers, C.B., van Krieken, J.H., van de Velde, C.J., and Verspaget, H.W. (2000). Superoxide dismutases in gastric and esophageal cancer and the prognostic impact in gastric cancer. Clin. Cancer Res. *6*, 3183–3192.

31. Iarc, L. (1994). Schistosomes, liver flukes and Helicobacter pylori. IARC Working Group on the Evaluation of Carcinogenic Risks to Humans. Lyon, 7-14 June 1994. IARC Monogr. Eval. Carcinog. Risks Hum. *61*, 1–241.

32. Zelko, I.N., Mariani, T.J., and Folz, R.J. (2002). Superoxide dismutase multigene family: a comparison of the CuZn-SOD (SOD1), Mn-SOD (SOD2), and EC-SOD (SOD3) gene structures, evolution, and expression. Free Radic. Biol. Med. *33*, 337–349.

33. Sbardella, D., Tundo, G.R., Mecchia, A., Palumbo, C., Atzori, M.G., Levati, L., Boccaccini, A., Caccuri, A.M., Cascio, P., Lacal, P.M., et al. (2022). A novel and atypical NF-KB pro-inflammatory program regulated by a CamKII-proteasome axis is involved in the early activation of Muller glia by high glucose. Cell Biosci. *12*, 108.

34. Fruehauf, J.P., and Meyskens, F.L., Jr. (2007). Reactive oxygen species: a breath of life or death? Clin. Cancer Res. *13*, 789–794.

35. Zhang, X., Liao, X., Wang, M., Liu, J., Han, J., An, D., Zheng, T., Wang, X., Cheng, H., and Liu, P. (2024). Inhibition of palmitoyltransferase ZDHHC12 sensitizes ovarian cancer cells to cisplatin through ROS-mediated mechanisms. Cancer Sci. *115*, 1170–1183.

36. Paku, M., Haraguchi, N., Takeda, M., Fujino, S., Ogino, T., Takahashi, H., Miyoshi, N., Uemura, M., Mizushima, T., Yamamoto, H., et al. (2021).

SIRT3-Mediated SOD2 and PGC-1α Contribute to Chemoresistance in Colorectal Cancer Cells. Ann. Surg. Oncol. *28*, 4720–4732.

37. Hart, P.C., Mao, M., de Abreu, A.L.P., Ansenberger-Fricano, K., Ekoue, D.N., Ganini, D., Kajdacsy-Balla, A., Diamond, A.M., Minshall, R.D., Consolaro, M.E.L., et al. (2015). MnSOD upregulation sustains the Warburg effect via mitochondrial ROS and AMPK-dependent signalling in cancer. Nat. Commun. *6*, 6053.

38. Wang, S., Chen, Z., Zhu, S., Lu, H., Peng, D., Soutto, M., Naz, H., Peek, R., Jr., Xu, H., Zaika, A., et al. (2020). PRDX2 protects against oxidative stress induced by H. pylori and promotes resistance to cisplatin in gastric cancer. Redox Biol. *28*, 101319.

39. Wen, J., Wang, Y., Gao, C., Zhang, G., You, Q., Zhang, W., Zhang, Z., Wang, S., Peng, G., and Shen, L. (2018). Helicobacter pylori infection promotes Aquaporin 3 expression via the ROS-HIF-1α-AQP3-ROS loop in stomach mucosa: a potential novel mechanism for cancer pathogenesis. Oncogene *37*, 3549–3561.

40. Feng, L., Zhao, K., Sun, L., Yin, X., Zhang, J., Liu, C., and Li, B. (2021). SLC7A11 regulated by NRF2 modulates esophageal squamous cell carcinoma radiosensitivity by inhibiting ferroptosis. J. Transl. Med. *19*, 367.

41. Zuo, S., Yu, J., Pan, H., and Lu, L. (2020). Novel insights on targeting ferroptosis in cancer therapy. Biomark. Res. *8*, 50.

42. Sharma, P., Shimura, T., Banwait, J.K., and Goel, A. (2020). Andrographis-mediated chemosensitization through activation of ferroptosis and suppression of β-catenin/Wnt-signaling pathways in colorectal cancer. Carcinogenesis *41*, 1385–1394.

43. Duan, Y., Kong, P., Huang, M., Yan, Y., Dou, Y., Huang, B., Guo, J., Kang, W., Zhu, C., Wang, Y., et al. (2024). STAT3-mediated up-regulation of DAB2 via SRC-YAP1 signaling axis promotes Helicobacter pylori-driven gastric tumorigenesis. Biomark. Res. *12*, 33.

44. Li, T., Fu, J., Zeng, Z., Cohen, D., Li, J., Chen, Q., Li, B., and Liu, X.S. (2020). TIMER2.0 for analysis of tumor-infiltrating immune cells. Nucleic. Acids Res. *48*. W509-w514.

45. Bartha, Á., and andGyőrffy, B. (2021). TNMplot.com: A Web Tool for the Comparison of Gene Expression in Normal, Tumor and Metastatic Tissues. Int. J. Mol. Sci. *22*, 2622.

46. Duan, Y., Yan, Y., Fu, H., Dong, Y., Li, K., Ye, Z., Dou, Y., Huang, B., Kang, W., Wei, G.H., et al. (2024). SNHG15-mediated feedback loop interplays with HNRNPA1/SLC7A11/GPX4 pathway to promote gastric cancer progression. Cancer Sci. *115*, 2269–2285.

47. Schneider, C.A., Rasband, W.S., and Eliceiri, K.W. (2012). NIH Image to ImageJ: 25 years of image analysis. Nat. Methods *9*, 671–675.

48. Zhang, L., Lu, X., Xu, Y., La, X., Tian, J., Li, A., Li, H., Wu, C., Xi, Y., Song, G., et al. (2023). Tumor-associated macrophages confer colorectal cancer 5-fluorouracil resistance by promoting MRP1 membrane translocation via an intercellular CXCL17/CXCL22-CCR4-ATF6-GRP78 axis. Cell Death Dis. *14*, 582.

49. Zhu, S., Soutto, M., Chen, Z., Peng, D., Romero-Gallo, J., Krishna, U.S., Belkhiri, A., Washington, M.K., Peek, R., and El-Rifai, W. (2017). Helicobacter pylori-induced cell death is counteracted by NF-κB-mediated transcription of DARPP-32. Gut *66*, 761–762.

50. Guo, L., Mohanty, A., Singhal, S., Srivastava, S., Nam, A., Warden, C., Ramisetty, S., Yuan, Y.C., Cho, H., Wu, X., et al. (2023). Targeting ITGB4/SOX2-driven lung cancer stem cells using proteasome inhibitors. iScience *26*, 107302.

51. Mo, Y., Zhu, J.L., Jiang, A., Zhao, J., Ye, L., and Han, B. (2019). Compound 13 activates AMPK-Nrf2 signaling to protect neuronal cells from oxygen glucose deprivation-reoxygenation. Aging *11*, 12032–12042.

52. Esteban, M.A., Wang, T., Qin, B., Yang, J., Qin, D., Cai, J., Li, W., Weng, Z., Chen, J., Ni, S., et al. (2010). Vitamin C enhances the generation of mouse and human induced pluripotent stem cells. Cell Stem Cell *6*, 71–79.

STAR★METHODS

KEY RESOURCES TABLE

REAGENT or RESOURCE	SOURCE	IDENTIFIER
Antibodies		
anti-SOD2	Cell Signaling Technology	Cat# 13141; RRID: AB_2636921
anti-CagA	Santa Cruz Biotechnology	Cat# sc-28368; RRID: AB_628229
anti-p65	Cell Signaling Technology	Cat# 8242; RRID: AB_10859369
anti-Phospho-p65(Ser536)	Cell Signaling Technology	Cat# 3033; RRID: AB_331284
anti-AKT	Cell Signaling Technology	Cat# 4685; RRID: AB_2225340
anti-Phospho-AKT (Ser473)	Cell Signaling Technology	Cat# 4060; RRID: AB_2315049
anti-4-hydroxy-2-nonenal	Abcam	Cat# ab46545; RRID: AB_722490
anti-SOD2 (acetyl K122)	Abcam	Cat# ab214675; RRID: AB_2892634
anti-SOD2 (acetyl K68)	Abcam	Cat# ab137037; RRID: AB_2784527
anti-HSC70	Proteintech	Cat# 10654-1-AP; RRID: AB_2120153
anti-GPX4	Proteintech	Cat# 67763-1-Ig; RRID: AB_2909469
anti-GAPDH	Cell Signaling Technology	Cat# 5174; RRID: AB_10622025
anti-rabbit IgG	Millipore	Cat# AP132; RRID: AB_92486
Bacterial and virus strains		
Helicobacter pylori strain 26695	ATCC	*Helicobacter pylori* strain 26695 [KE26695]
Helicobacter pylori strain 43504	ATCC	*Helicobacter pylori* strain NCTC 11637
Helicobacter pylori strain PMSS1	Lab stored; Yantao Duan; Fudan University[43]	N/A
Lentivirus	This paper	N/A
Biological samples		
Human tissue samples	Changzheng Hospital of Navy Medical University	N/A
Gastric tissue in mice	This paper	N/A
Chemicals, peptides, and recombinant proteins		
5-fluorouracil	Beyotime	Cat# ST1060
MK2206	Beyotime	Cat# SF2712
NF-κB inhibitor Bay 11–7082	Selleckchem	Cat# S2913
Erastin	univ-bio	Cat# abs810744
Ferrostatin-1	univ-bio	Cat# abs813072
Recombinant human tumor necrosis factor (TNF)-α	PeproTech	Cat# 300-01A
FBS	Gibco	Cat# 10099-141
PBS	Sangon Biotech	Cat# A610100
TRIzol reagent	Ambion	Cat# 15596018
DMSO	Merck	Cat# D2650
PVDF membrane	Millipore	Cat# IEVH00005
DAPI	Beyotime	Cat# C1002
RPMI-1640	Gibco	Cat# 11875119
DMEM	Gibco	Cat# 12491015
RIPA lysis buffer	Beyotime	Cat# P0013B
Brain heart infusion agar	Thermo Fisher Scientific	Cat# 6105300
Sheep blood	Solarbio	Cat# TX0030
Puromycin	Beyotime	Cat# ST551
Crystal violet	Beyotime	Cat# C0121
protein A/G magnetic beads	Millipore	Cat# 16-663

(Continued on next page)

Continued

REAGENT or RESOURCE	SOURCE	IDENTIFIER
Critical commercial assays		
Cell Counting Kit-8	DOJINDO	Cat# CK04
Lipofectamine™ 3000 transfection kit	Thermo Fisher Scientific	Cat# L3000150
Illumina HiSeq 2500 Analyzer	Illumina	N/A
Clarity™ Western ECL Substrate	Bio-Rad	Cat# 1705060
iScript™ cDNA synthesis kit	Bio-Rad	Cat# 1708891
iTaq Universal SYBR Green Supermix	Bio-Rad	Cat# 1725125
Superoxide assay kit	Beyotime	Cat# S0060
Reactive Oxygen Species Assay Kit	Beyotime	Cat# S0033S
Lipid Peroxidation Assay Kits	Beyotime	Cat# S0043S
Dual-Luciferase Assay	Promega	Cat# E1910
Deposited data		
TIMER	Li et al.[44]	http://timer.cistrome.org/
TNMplot	Bartha et al.[45]	http://www.kmplot.com
Gene Expression Omnibus (GEO)	This paper	GSE278591
Experimental models: Cell lines		
Human gastric cancer cell line AGS	ATCC	Duan et al.[43]
Human gastric cancer cell line BGC823	ATCC	Duan et al.[46]
Human gastric cancer cell line HGC27	Shanghai Institutes for Biological Sciences	Duan et al.[43]
Human gastric cancer cell line MGC803	Shanghai Institutes for Biological Sciences	Duan et al.[46]
Human gastric cancer cell line MKN45	Shanghai Institutes for Biological Sciences	Duan et al.[43]
Normal gastric epithelial cells GES1	Shanghai Institutes for Biological Sciences	Duan et al.[46]
Human Embryonic Kidney 293T	ATCC	Cat# CRL-3216
Experimental models: Organisms/strains		
C57BL/6 mice	SLAC LABORATORY ANIMAL	N/A
BALB/c nude mice	SLAC LABORATORY ANIMAL	N/A
Oligonucleotides		
siRNA1 for SOD2: GUGGUGGUCAUAUCAAUCAUU	GenePharma	N/A
siRNA2 for SOD2: GUGGUGGUCAUAUCAAUCAUU	GenePharma	N/A
siRNA1 for HSC70: GGAGAGUCCUUGCAUAGAC	GenePharma	N/A
siRNA2 for HSC70: GUGCUGAUCAUAUCAAUCAUU	GenePharma	N/A
SOD2 shRNA: GATCCCGGGGGTTGGCTTGGTTTCAATATTCAAGAGATATTGAAACCAAGCCAACCCCTTTTTA	This paper	N/A
Primers for qPCR, see Table S2	This paper	N/A
CHIP primers for the NF-κB binding sites, see Table S3	This paper	N/A
Recombinant DNA		
pcDNA3.1 plasmid: SOD2	Invitrogen	N/A
pRL-TK	Promega	Cat# E2241
pGL3-Basic vector	Promega	N/A
Software and algorithms		
ImageJ software	Schneider et al.[47]	https://imagej.net/software/fiji/
Adobe Photoshop Adobe	Adobe Photoshop Adobe	https://www.adobe.com/es/
Graphpad Prism 8	GraphPad Prism Software, Inc	https://www.graphpad.com/
R language	The R Project for Statistical Computing	https://www.r-project.org/

EXPERIMENTAL MODEL AND STUDY PARTICIPANT DETAILS

Mouse models

All animal experiments were reviewed and approved by the Institutional Animal Care and Use Committee of Naval Medical University (2023079). Mice were housed in a specific-pathogen-free animal laboratory in 12 h light–dark cycles. Twenty 6-week-old male C57BL/6 mice (SLAC LABORATORY ANIMAL, Shanghai, China) were randomly assigned into the control and PMSS1 groups with 10 mice per group. *H. pylori* strain PMSS1 of 10^9 colony-forming unit (CFU)/mouse was used for orogastric gavage, while the control mice were treated with Brucella broth. Two weeks later, mice were euthanized, and the gastric tissues were used for western blot and qRT-PCR analysis.

MGC803 cells with stable knockdown of SOD2 (scrambled or shSOD2) were subcutaneously injected into four-week-old male BALB/c nude mice (SLAC LABORATORY ANIMAL, Shanghai, China). When the average tumor volume reached approximately 100 mm^3, the mice were were randomly divided into four groups and injected intraperitoneally with 5-FU at a dose of 20 mg/kg every two days. The control group mice were injected with saline. Mice were sacrificed and examined for tumor growth four weeks after injection. The tumor length (L) and width (W) were measured using a digital caliper twice per week after inoculation. The tumor volume was calculated as follows: $V = L \times W^2 \times 0.5$.[48]

Cell culture and reagents

Human GC cell lines AGS and BGC823 were obtained from ATCC (Manassas, VA, USA). The HGC27, MGC803, MKN45, and GES1 cell lines were purchased from Shanghai Institutes for Biological Sciences, Chinese Academy of Sciences. The cell lines were authenticated by short tandem repeat-based assay. AGS, BGC823, MKN45, and HGC27 cells were cultured in RPMI-1640 medium with 10% fetal bovine serum (FBS) at 37°C in a humidified atmosphere containing 5% CO_2. MGC803 and GES1 cells were cultured in Dulbecco's Modified Eagle Medium (DMEM) with 10% FBS at 37°C in a humidified atmosphere of 5% CO_2. Recombinant human tumor necrosis factor (TNF)-α (#300-01A, PeproTech, NJ, USA), 5-fluorouracil (5-FU) (#ST1060, Beyotime, Shanghai, China), MK2206 (#SF2712, Beyotime, Shanghai, China) and NF-κB inhibitor Bay 11–7082 (#S2913, Selleckchem, Houston, TX, USA) were purchased. Erastin (#abs810744) and ferrostatin-1 (#abs813072) were obtained from univ-bio (Shanghai, China). The final concentrations used in the experiments were as follows: ferrostatin-1, 2 μM; and erastin, 20 μM.

METHOD DETAILS

Patient samples and ethical statement

This study enrolled a total of sixty-five GC patients from January 2016 to December 2018 at the Department of General Surgery, Changzheng Hospital, Navy Medical University, Shanghai, China. The clinical and demographic information of the study participants was shown in Table S1. All patients were pathologically diagnosed with GC in accordance with the American Joint Committee on Cancer criteria. This study was approved by the by the Human Research Ethics Committee of Changzheng Hospital, Navy Medical University (2023SL068). This study was also conducted in accordance with the Declaration of Helsinki. Informed consent was provided by all enrolled patients. TIMER and TNMplot, two interactive web servers, were used to compare the expression levels of SOD2 in The Cancer Genome Atlas (TCGA)-STAD cohort with adjacent normal TCGA samples. The GSE60427 dataset included 8 normal and 24 *H pylori*-positive specimens from gastric mucosal biopsies and was obtained from the Gene Expression Omnibus (GEO) database (https://www.ncbi.nlm.nih.gov/geo/). The animal experiments were approved by the Institutional Animal Care and Use Committee of Naval Medical University (2023079), in accordance with the Guide for the U.S. Public Health Service's policy on laboratory animals.

Immunohistochemistry (IHC) and immunofluorescence

Paraffin-embedded clinical samples were used for immunostaining to detect SOD2 protein expression. In brief, tumor tissues were fixed with 4% (v/v) formaldehyde, embedded in paraffin, and cut into 5 μm thick sections. The sections were incubated with the primary antibody against SOD2 (1:500; #13141S, Cell Signaling Technology) overnight at 4°C in a moist chamber. The sections were incubated with HRP-conjugated secondary antibody for 15 min at room temperature, and then stained with DAB and hematoxylin. The IHC results were scanned by whole-slide scanning Pannoramic scanner (3D HISTECH, Waltham, MA, USA). The protein expression levels were tested and scored based on intensity and frequency.[49]

Immunofluorescence staining was performed as described previously.[50] Fixed and permeabilized gastric mucosa tissues were permeabilized with 0.5% Triton X-100, and then blocked with 10% BSA. The tissues were incubated with primary antibodies at room temperature for 2 h, followed by incubation with fluorescent dye-labeled secondary antibodies at room temperature for 2 h. DAPI was used to stain the nuclei (Beyotime, Shanghai, China). The stained cells were imaged with a Leica TCS SP8 Inverted Fluorescence Microscope (Leica Microsystems).

H. pylori culture and infection

Wild-type Cag$^+$ *H. pylori* strains 26695 and 43504 were obtained from ATCC, and the rodent-adapted PMSS1 was stored in our laboratory. Briefly, *H. pylori* strains were maintained in brain heart infusion agar (OXOID, Thermo Fisher Scientific, USA) with 10% sheep

blood. Subsequently, the strains were cultured at 37°C and placed in an incubator with 85% N_2, 5% O_2, and 10% CO_2 for 16 h. *H. pylori* were co-cultured with GC cells at a multiplicity of infection (MOI) of 100.

RNA sequencing analysis (RNA-seq)

Next-generation RNA sequencing analysis was applied to test the mRNA expression features by Illumina HiSeq 2500 (Illumina, San Diego, CA, USA). Significant differential expression of a gene was identified as a > 2-fold difference between treatment and control samples with a *p* value <0.05. The heatmap was visualized by Gene Ontology (GO) using Cluster software. Differentially expressed genes (DEGs) were analyzed using GO analysis. Finally, Kyoto Encyclopedia of Genes and Genomes (KEGG) annotations were performed to analyze the enrichment of DEGs.

RNA interference, plasmid construction, and transfection

Two synthesized duplex small interfering RNA oligos (siRNAs) were synthesized for each target gene from GenePharma (Shanghai, China). The SOD2 siRNAs at a final concentration of 100 nmol/L were transfected into GC cells using the Lipofectamine 3000 transfection kit (Thermo Fisher Scientific) in accordance with the manufacturer's instructions. The coding sequence of SOD2 was cloned in pcDNA3.1 plasmid (Invitrogen). Human SOD2 knockdown and control plasmids were transfected into GC cells by Lipofectamine 3000 reagent in accordance with the manufacturer's instructions. This construct was then cotransfected with pGAG and pVSVG into HEK293T cells. Retroviral supernatant medium was used to infect MGC803 cells. The virus-infected cells were selected using 2 μg/mL puromycin for 2 weeks.

Western blot and immunoprecipitation

Cells were washed with pre-cooled PBS and lysed using RIPA buffer. Lysates were then centrifuged at 13,000 rpm for 10 min at 4°C. For immunoprecipitation experiments, the lysate containing 500 μg protein was incubated with 2 μg primary antibody at 4°C. The immune complexes were captured using protein A/G agarose beads. The beads were washed three times in TBST, and then the immunoprecipitated proteins were resuspended in SDS-PAGE sample loading buffer, followed by western blot analysis. Briefly, proteins were separated by 10% SDS-PAGE and transferred to a PVDF membrane (Millipore). We then incubated the blots with primary antibodies specific to SOD2 (1:1000; #13141S, Cell Signaling Technology), CagA (1:300; #sc-28368, Santa Cruz Biotechnology), p65 (1:1000; #8242S, Cell Signaling Technology), p-p65 (1:1000; #3033S, Cell Signaling Technology), AKT (1:1000; #4685S, Cell Signaling Technology), *p*-AKT (1:1000; #4060S, Cell Signaling Technology), 4-hydroxy-2-nonenal (4-HNE) (1:1000; #ab46545, Abcam), SOD2 (acetyl K122) (1:1000; #ab214675, Abcam), SOD2 (acetyl K68) (1:1000; #ab137037, Abcam), HSC70 (1:1000; #10654-1-AP, Proteintech) or GPX4 (1:1000; #67763-1-Ig, Proteintech) overnight at 4°C. The blots were then incubated with the appropriate species-specific secondary antibody for 1 h at room temperature. GAPDH (1:1000; #5174S, Cell Signaling Technology) was used as the loading control. The blot analysis was visualized by the Clarity Western ECL Substrate (Bio-Rad, #1705060). Protein band analysis was done using ImageJ software.

Quantitative real-time PCR

Isolation of total RNA was performed using TRIzol reagent (Ambion, # 15596018). Total RNA (1 μg) was reverse transcribed by an iScript cDNA synthesis kit (Bio-Rad, CA, USA). cDNA was used to analyze the mRNA levels of SOD2 by qRT-PCR assay using iTaq Universal SYBR Green Supermix (Bio-Rad). The sequences of RT-qPCR primers are shown in Table S2. Each reaction was performed in triplicate. The relative expression levels of genes were analyzed by the $2^{-\Delta\Delta Ct}$ method. GAPDH was used as a normalization control.

Cell viability assay

Ten thousand cells were seeded in a 96-well plate and treated with erastin, ferrostatin-1, or dimethyl sulfoxide (DMSO) for 12 h. Then, 100 μL of medium containing 10% CCK-8 reagent was added in accordance with the manufacturer's instructions (Dojindo, Kumamoto, Japan). Each group had three duplicate wells. Following incubation at 37°C for 1 h, the absorbance was then measured using a Safire[2] microplate reader (Tecan, Switzerland) at 450 nm.

For cell viability analysis, 10^6 GC cells/well were seeded on six-well plates. Cells were treated with erastin, ferrostatin-1, or DMSO for 12 h. The trypan blue exclusion staining assay was then used to evaluate the cell viability. Cell viability was detected using a cell viability analyzer (Beckman). All the experiments were conducted in triplicate.

Superoxide assay

The cellular superoxide contents were examined by a superoxide assay kit (Beyotime, Shanghai, China) following the referenced protocol.[51] GC cells with different treatments were incubated with the superoxide detection reagents for 30 min at room temperature. Subsequently, the absorbance was detected using a spectrophotometer (Thermo Fisher Scientific) (OD = 450 nm).

ROS assay

As previously described,[52] ROS concentrations were tested by a Reactive Oxygen Species Assay Kit (Beyotime, Shanghai, China). Following the applied treatment, GC cells were co-incubated with DCFH-DA for 30 min at 37°C and subsequently detected by fluorescence spectrophotometer (Thermo Fisher Scientific).

Lipid peroxidation assay

The malonic dialdehyde (MDA) concentrations of cell lysates were evaluated by Lipid Peroxidation Assay Kits (Beyotime, Shanghai, China) in accordance with the manufacturer's instructions. The assay detects the MDA-thiobarbituric acid (TBA) adducts generated by the reaction of MDA with TBA. The MDA-TBA adducts can be further measured using colorimetry.

Luciferase reporter assay

The specific sequences in the SOD2 promoter were acquired from the National Center for Biotechnology Information, and then subcloned into the pGL3-Basic vector (Promega, Madison, WI, USA) to construct luciferase reporter plasmids (P1: 1200-0 bp upstream of the SOD2 coding sequence, P2: 1000-0 bp upstream of the SOD2 coding sequence, P3: 600-0 bp upstream of the SOD2 coding sequence). For luciferase analysis, 293T cells were seeded in a 12-well plate and co-transfected with NF-κB expression vector and the luciferase plasmids for 24 h. Subsequently, cells were analyzed using a Dual-Luciferase Assay following the manufacturer's instructions (Promega). Each transfection was performed in triplicate.

Chromatin immunoprecipitation assay

MGC803 cells were crosslinked with 1% formaldehyde and resuspended in 400 μL lysis buffer. The crosslinked DNA was then sonicated into 200–500 bp fragments for the following DNA pull-down. The antibodies used for chromatin immunoprecipitation (ChIP) were as follows: NF-κB p65 (Ser536) (#3033S, Cell Signaling Technology), rabbit IgG (Millipore), and protein A/G magnetic beads (#CS204457, Millipore). These were added to the cell lysates and incubated at 4°C overnight. Elution of the immunoprecipitated chromatin complexes was followed by DNA purification, and then the purified DNA was further analyzed by PCR assays. The sequences of ChIP primers for the NF-κB binding sites are shown in Table S3.

Colony formation

Approximately 300 GC cells were seeded on six-well plates, infected with *H. pylori*, and cultured at 37°C and 5% CO_2 for 2 weeks. Briefly, GC cells were fixed with paraformaldehyde and dyed with 0.2% (w/v) crystal violet. Subsequently, images were acquired and the colonies were counted.

QUANTIFICATION AND STATISTICAL ANALYSIS

All data presented are representative of at least three independent experiments and expressed as the mean ± standard deviation (SD). The differences between groups were analyzed by one-way analysis of variance (ANOVA) and Student's t test. Overall survival (OS) was analyzed with the Kaplan–Meier method. Spearman correlation was used to determine the expression correlation of two genes. The sample size of mice was estimated by the degrees of freedom of ANOVA. All statistical analyses were conducted using SPSS 16.0 and GraphPad Prism 8.0. A two-tailed value of $p < 0.05$ was considered to be statistically significant.